

## Design, Analysis, of High Performance Antennas for 5G Communications Analysis Using WCIP

Anouar Mondir<sup>1, \*</sup>, Mohammed Ali Ennasar<sup>2</sup>, Larbi Setti<sup>1</sup>, and Figuigue Mustapha<sup>2</sup>

**Abstract**—This article presents the recent advancements in utilizing metamaterials for the development of high-performance antennas in 5G communications. The focus is on negative refractive index metamaterials composed of two unit cells: a complementary infinite split ring resonator (CI-SRR) and a Hilbert fractal embedded in the ground plane. These metamaterials enable antenna size reduction while enhancing performance. The proposed antenna metamaterials offer improved antenna characteristics and precise control over physical dimensions, facilitating the creation of highly efficient devices with miniaturized antennas. Additionally, an antenna array  $1 \times 3$  is incorporated to further enhance performance. The antenna design has a compact size of  $40 \times 33 \times 1.57 \text{ mm}^2$  and is fabricated using Rogers RT/Duroid 5880 material. The final broadband antenna exhibits a wide impedance bandwidth of 12.71% at 32 GHz, accompanied by a gain of 10.5 dBi. The comparison between wave concept iterative process (WCIP) calculations and measurements shows good agreement. The fabricated structure is thoroughly analyzed using a Keysight PNA network analyzer, demonstrating its successful operation and suitability for broadband applications.

### 1. INTRODUCTION

The increasing number of people using cell phones, tablets, and other portable wireless devices has accelerated the advancement of wireless communication technologies and systems. Specifically, for wireless communications, which require a lightweight, high-gain antenna for improved system performance, the compression antenna must have a high gain and wide bandwidth to meet the growing demand for superior communication quality with millions of users [1]. The use of a single-patch printed antenna is often insufficient to meet the imposed radiation constraints. Specific characteristics such as high gain or a shaped main lobe can be usually only achieved by grouping several radiating sources to form a system called an antenna array [2]. The advantage of assembling several primary antennas is that highly directed radiation can be obtained, depending on the number and nature of the elements, the form of their power supply, and their technical arrangement in the array [2, 3]. 5G will offer greater throughput, although it remains difficult to accurately estimate the gain for the end consumer [4].

The size of the radio frequency (RF) front-end circuit that powers the antenna element is comparable to the small footprint of the antenna elements at millimeter-wave frequencies. The radio front ends and millimeter wave antennas can coexist on the same chip. As a result, there is no longer a need for intricate, low-loss RF interconnects to connect the device to an additional antenna substrate. On-chip antennas, however, have very low efficiency as a result of the high permittivity of the substrate and general high doping levels. Because the properties of the substrate are already intimately linked to the technology of the integrated circuit being utilized, it is frequently not viable to alter them to lessen this effect. Scaling of on-chip antennas appears doomed, with the exception of low-performance,

---

*Received 22 May 2023, Accepted 14 July 2023, Scheduled 6 August 2023*

\* Corresponding author: Anouar Mondir (mondir.anouar@uae.ac.ma).

<sup>1</sup> LSTA, FPL, Abdelmalek Essaadi University, Tetouan, Morocco. <sup>2</sup> Laboratoire System of Information and Telecommunications (LaSIT), Faculty of Science, Abdelmalek Essaadi University, Tetouan, Morocco.

low-cost solutions used in older integrated circuit technologies, since the cost of chip area (measured in cents/mm<sup>2</sup>) rises with each iteration of integrated circuit technology. Integrated antennas, which combine an antenna substrate and a front-end RF chip in a single package, are significantly more efficient than on-chip antennas but cost more due to complex packaging procedures. The antenna aperture is maintained at higher frequencies in larger antenna arrays. As a result, the directivity increases, requiring the use of phased array antennas or more general beamforming architectures to create antenna arrays capable of electrically steering the beam direction.

In recent years, many microstrip antenna arrays have been developed and studied. The authors of [5] proposed an antenna array based on substrate-integrated waveguide technology working at Ka-band (29.35 GHz) with a gain, 8.1 dB bandwidth of 0.351 GHz. In this work, [6], a  $2 \times 2$  array patch antenna for 5G with two slots covering the C-band (3.4–3.6 GHz) with a bandwidth of 0.2 GHz and bandwidth of 5.37 dBi. In [7], the authors proposed an antenna comprising an 8-element array with a high impedance matching feed array working at a multi-band frequency that enhances the gain and bandwidth. In [8], an antenna array for 5G mobile operates at dual-bands (28 GHz and 24.9 GHz) with a gain of 8.42 dBi, 5.375 dBi, and bandwidth of 0.9 GHz, 0.3 GHz, respectively. In this paper [9], a 4-element compact slot antenna array is developed for 5G applications with a slot length of 4.01 mm, a peak gain of 9.25 dB at 26.9 GHz, and a bandwidth of 1.27 GHz. This paper [10] proposed a T-slot shape on the patch, and the built antenna can be incorporated into a 5G communication device. This antenna has two operating frequencies of 2.34 GHz and 25.4 GHz while peak gains are about 2.82 dB and 9.65 dB. The gain of an antenna can be improved by different methods, like an array antenna, adding a periodic structure in the ground plane, etc. All antennas examined so far are suitable for 5G communications; however, these antennas have poor gain values and a limited bandwidth [11].

Researchers have shown increased interest in the development of metamaterials [12]. Metamaterials are attracting a lot of attention for different microwave applications because of their properties that do not exist in nature. An effectively homogeneous artificial electromagnetic structure is employed in some applications like filters [13], microwave applications [14], and antennas [15]. The physicist Victor Veselago has described that such a material would have properties that would allow the inversion of the Snell-Descartes law of refraction, the inversion of the Doppler effect, and the inversion of Cerenkov radiation [16, 17]. The application of these materials in antennas allows for performance improvements such as gain, efficiency, bandwidth, and size reduction [18]. Split ring resonator and complementary split ring resonator are the most often used metamaterials. They offer negative permeability and permittivity, respectively, and have the same resonance frequency for the same size.

Metamaterials are employed in antenna geometry to improve antenna properties, including impedance matching and gain, according to Lizzi et al. in [19]. In order to operate at 2.48 GHz and lower the size of the antenna geometry, Laila et al. developed the complementary multi-ring SRR in the ground plane employing a circular-shaped radiating patch in [20]. It reduces mutual coupling by overcoming surface wave propagation. Renowned researchers have researched different types of SRR-inspired antennas, where the ground plane is designed in the shape of an SRR by Hu and LI [21], creating fractal geometry by repeating SRRs, etc. Cao et al. [22], which has a high gain value, compared a loaded SRR antenna with an unloaded SRR antenna and revealed that the loaded SRR antenna has a high gain and improved bandwidth, which illustrated the SRR-inspired periodic end-fire antenna. The authors in [23] proposed a metamaterial-inspired circularly polarized broadband slot antenna loaded by SRR. The authors used SRR to change the frequency and miniaturize the proposed antenna. Kuhestani et al. [24] developed a compact metamaterial-based patch antenna with circular polarization for WiMAX applications. Sharma and Bhatia [25] demonstrated an antenna for SRR-based multistandard wireless applications employing a radiating fidget spinner patch. Patel et al. [26] proposed a metamaterial-based reconfigurable antenna using a rectangle-shaped SRR with three rings; the gain was enhanced to 16.71 dBi from 4.47 dBi using multiple commutation states with the metamaterial. Sharma and Bhatia [27] introduced a parasitic edge-coupled split-ring resonator in a low-cost fractal antenna geometry for multiband wireless applications. The authors in [28] included the loading of the suggested antenna with SRR, the effects of the parasitic Edge-Coupled (EC) structure. The authors of [29] have presented configurations that utilize Hilbert fractal curves to enable the miniaturization of artificial magnetic materials, resulting in enhanced homogeneity and reduced substrate profile. The concept of using fractal curves to scale down artificial magnetic materials was proposed. The first

mention of this idea was made in a conference article in [30]. While Euclidean geometry is limited to points, lines, surfaces, and volumes, fractals include geometric shapes that fall in between [29, 30]. Therefore, a fractal can be a line that reaches the surface. The line can be folded so that it effectively fills almost the entire surface. The self-filling properties of space result in curves that are electrically very long but fall into a small space. This characteristic can make the antenna elements smaller. In the previous section, it was mentioned that pre-fractals reduce the complexity of fractal geometry, which has not been recognized for specific applications. For antennas, this may mean that curves, which are much smaller than the wavelength of the frequency band used, may be blocked [31–34]. This makes the infinitely complex structure, which can only be analyzed mathematically, not physically created [35]. However, the number of iterations needed to obtain the benefits of miniaturization is limited to a few, before there are hard-to-distinguish complexities in the structure thus created [36]. Not yet released are many interesting works that concern the emerging field of fractal electrodynamics. The self-filling properties of Hilbert fractals have been demonstrated in [37] as an effective method to develop a compact resonant antenna. It is noted that most of the previous papers were based on new methods, but they are complex and expensive.

To achieve high bandwidth with a small antenna size compared to the references listed above, the dielectric substrate used is Rogers RT/Duroid 5880, which has the following properties: loss tangent ( $\tan(\delta) = 0.02$ ), thickness  $h = 1.57$  mm, and relative permittivity  $\epsilon_r = 2.2$ . The simulation and measurement results are well aligned. The main objective of this study is to examine how the performance of an antenna changes with parameters and to propose an improved design with high bandwidth, a small footprint, and high gain for 5G applications at 32 GHz. To reach these objectives, the WCIP approach, an iterative full-wave formulation based on the incidence and reflection of waves at the antenna interfaces, is used to analyze the proposed geometry. Following the identification of an antenna parameter, a new antenna shape with a wide bandwidth, high gain, and resonant frequency of 32 GHz is proposed. The WCIP approach is explained in Section 2. Section 3 presents the proposed antenna geometry and simulation results. Section 4 presents the measurement data of the prototype antenna and comparisons with the numerical results. Section 5 summarizes the conclusion.

## 2. WCIP FORMULATION

The relation between the incident wave  $\vec{A}_i$  and reflected wave  $\vec{B}_i$ , depicted in Figure 1, is the basis for the WCIP analysis. These, as shown in Equations (1) and (2) [15, 19], are represented by the tangential components of the electric field,  $\vec{E}_i$  the surface current densities,  $\vec{J}_i$  and  $Z_{01}$ , which is the characteristic impedance of the dielectric substrate.

$$\vec{A}_i = \frac{1}{2\sqrt{Z_{01}}} (\vec{E}_i + Z_{01}\vec{J}_i) \quad (1)$$

$$\vec{B}_i = \frac{1}{2\sqrt{Z_{01}}} (\vec{E}_i - Z_{01}\vec{J}_i) \quad (2)$$

The spatial domain and modal domain are the two domains in which the  $h$  analysis is performed. It is an iterative process based on the ratios of the incident and reflected wave components, which are determined at each iteration using Equations (3) and (4).

$$\vec{B}_i^n = \hat{S}\vec{A}_i^n + \vec{A}_0^n \quad (3)$$

$$\vec{A}_i^n = \hat{\Gamma}\vec{B}_i^n \quad (4)$$

In Equation (3),  $i$  is the dielectric or conductor medium,  $n$  the number of iterations, and  $\hat{S}$  the behavior of the electromagnetic (EM) wave incident on the surface of the structure in the spatial domain.  $\hat{\Gamma}$  is also the relationship at the interface of two dielectrics, and is considered in the spectral domain. The modal Fourier transform (FMT) is used in all iterations to convert the spatial domain to the modal domain [15, 17]. The generalized WCIP approach, which was created for the study of frequency selective surfaces (FSSs) with dissimilar array elements, is extended to produce results for the suggested antenna with two different elements (Figure 1). Decoupling between the sources and the resonant components

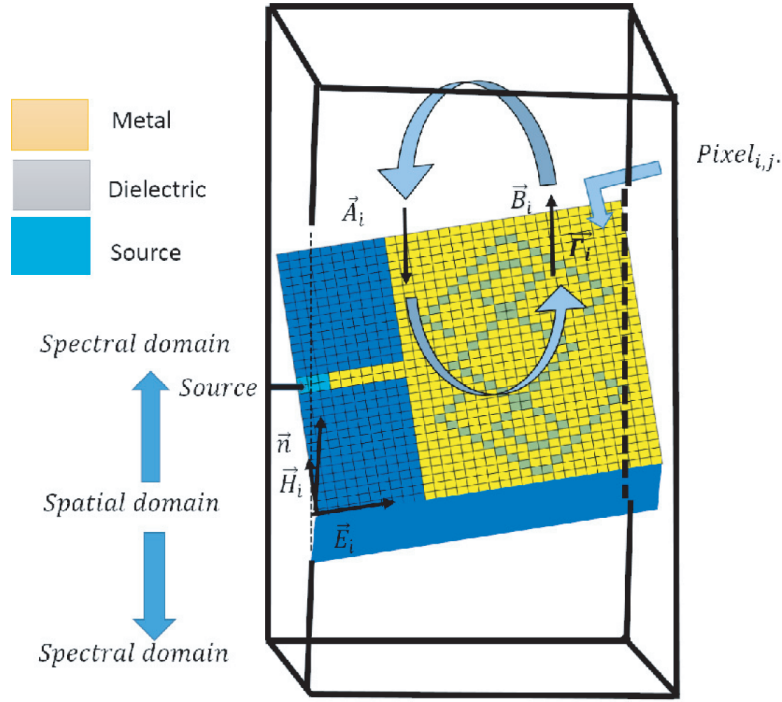


**Figure 1.** Wave propagation in planar antenna proposed.

is considered in this analysis. The modification is made to the scattering operator,  $\hat{S}$ , which is specified in the spatial domain (Figure 1).

Based on the equivalent electric field components, the sources are modeled while respecting the boundary conditions of the building sidewalls. Linearly polarized sources were considered to feed the patches, with a localized source modeled in a single direction. Here, only a small portion of the modeled space in the spatial domain is the location where the source is defined. At the circuit interface, the spreading operator can be generalized as described in [20, 21] by combining all incident and reflected wave relationships for each of the subdomains of each pixel (metal, dielectric, and source).

### 3. MODELING OF ANTENNA DESIGNS

#### 3.1. Unit Cell Description

In the study [38], the application of fractal curves to miniaturize antennas was investigated. The ideas can be applied to the design of small, low-profile antennas with an artificial magnetic material ground plane. By using full-wave modeling and experimental characterization, [39] has validated the analytical design. The antenna is reduced even further in size when higher-order Hilbert curves are used. Compared to specific square spiral inclusions, the new designs have better electromagnetic properties in terms of decreased frequency dispersion and lower magnetic loss at the resonant frequency. According to [40], this benefit is obtained at the expense of reduced permeability and increased magnetic loss at frequencies below resonance.

A complementary infinite split ring resonator (CI-SRR) is shown in Figure 2(a), which is magnetically resonant and attempts to achieve a vertical magnetic field, and this magnetic vertical field employs negative permittivity values. The index of refraction of an electromagnetically responsive material depends primarily on its permittivity and permeability, as indicated in the following:

$$n = \mp \sqrt{\epsilon\mu} \quad (5)$$

When the two parameters are negative, the refractive index is negative, which makes the waves propagate backward. Materials whose permittivity and permeability are simultaneously negative are

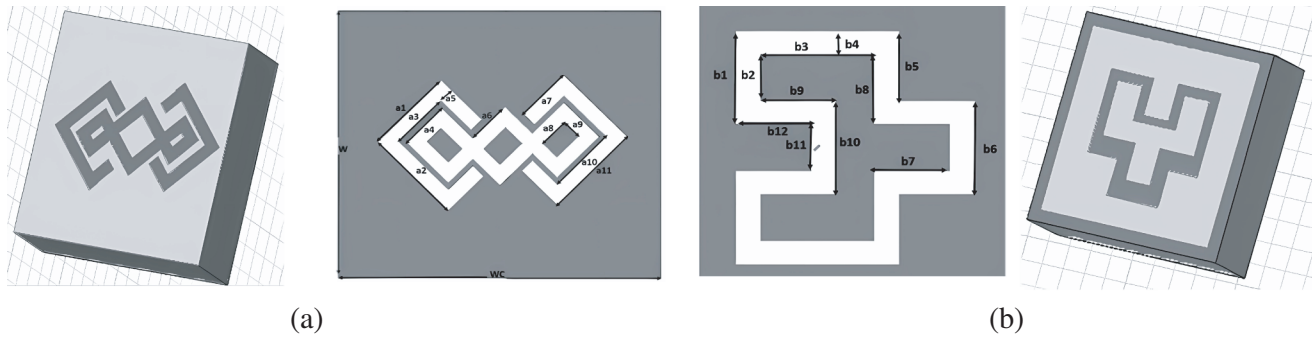


**Figure 2.** Unit cell with a (a) complementary infinite split and (b) Hilbert fractal.

called negative index materials (NIMs). They are also called left-handed materials. The values of  $\mu_{eff}$ ,  $\epsilon_{eff}$ ,  $N_{eff}$ , and  $z_{eff}$  were generated using a MATLAB algorithm. The permeability is determined by the following equation.

$$\mu = nz \tag{6}$$

where  $n$  is the index of refraction, and  $Z$  is the impedance. The relationships below relate the  $S$ -parameters to the refractive index and the impedance.

$$n = \frac{1}{kt} \cos^{-1} \left[ \frac{1}{2S_{21}} (1 - S_{11}^2 + S_{21}^2) \right] \tag{7}$$

$$z = \left[ \frac{(1 + S_{11})^2 - S_{21}^2}{(1 - S_{11})^2 - S_{21}^2} \right] \tag{8}$$

The dimensions of the suggested complementary infinity split ring resonator (CI-SRR) and Hilbert fractal are indicated in Table 1. It is excited by two ports along the  $Y$ -axis, a perfect magnetic conductor (PMC) along the  $Z$ -axis and a perfect electric conductor (PEC) along the  $X$ -axis.

**Table 1.** Dimension of the unit cell of the patch proposed.

Parameters	Values (mm)						
$a_1$	4	$b_1$	4	$a_7$	2	$b_7$	3
$a_2$	3.6	$b_2$	2	$a_8$	1.2	$b_8$	4
$a_3$	2.4	$b_3$	4	$a_9$	0.8	$b_9$	3
$a_4$	2	$b_4$	1	$a_{10}$	2.8	$b_{10}$	4
$a_5$	0.5	$b_5$	3	$a_{11}$	4	$b_{11}$	2
$a_6$	1.54	$b_6$	3	$W$	10.1	$W_c$	13

An iterative numerical simulation program was designed using MATLAB based on the WCIP method, for the modeling of materials and the calculation of the  $S$ -parameters, coupled with a method of extraction of electromagnetic characteristics named Nicolson-Ross-Weir (NRW) used to calculate and extract the constitutive characteristics: the permeability, permittivity, and refractive index for each pattern studied and for each miniaturization step. The relative effective electrical permeability and magnetic permeability of the complementary infinite-split resonator and unit cell with Hilbert fractal are shown in Figures 3 and 6. The figures show that the values are negative. Figures 4 and 5 show the relative index and impedance of the complementary infinite-split resonator and unit cell, respectively.

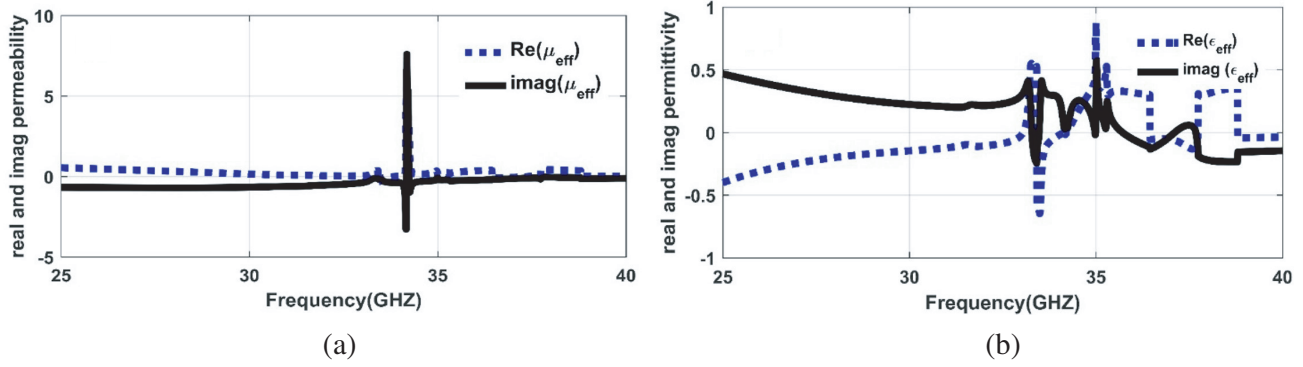


**Figure 3.** The simulated (a) the permeability, (b) the permittivity of the metamaterial unit cell *CI-SRR*.

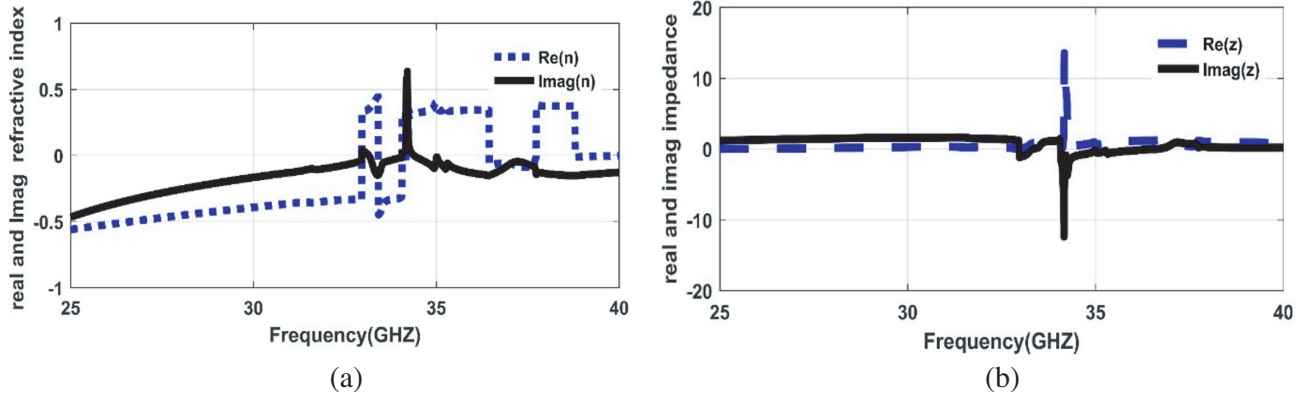


**Figure 4.** The simulated (a) the refractive index, (b) the impedance of the metamaterial unit cell *CI-SRR*.

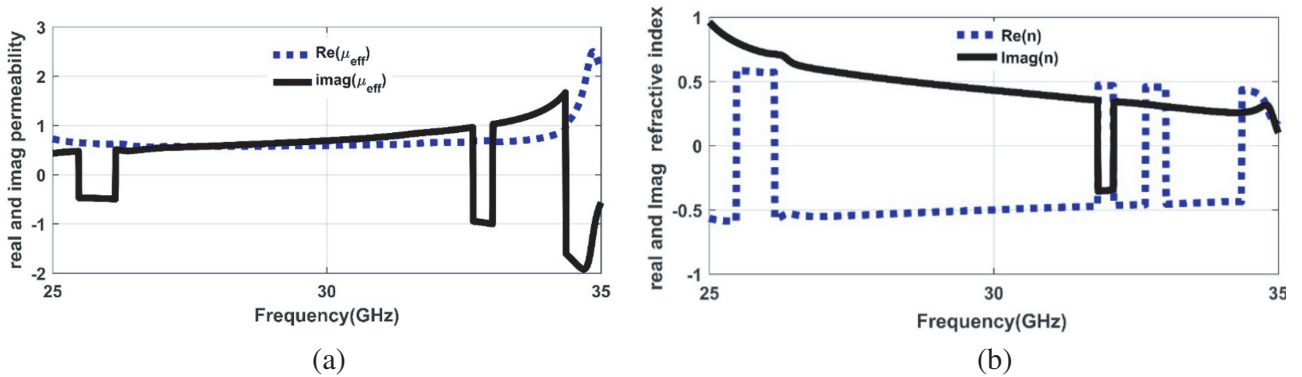


**Figure 5.** The simulated (a) the permeability, (b) the refractive index of the metamaterial unit cell Hilbert fractal.

The proposed miniature antenna structure is obtained by using a complementary infinite-split resonator and Hilbert fractal. The structure is common in a metasurface (MS) that is artificially generated to produce an anticipated magnetic predisposition in many types of MS up to 200 THz [42, 44]. The number of Hilbert fractals produces a capacitance that controls the resonance of the structure. The structure proposed in this paper is a combination of several *CI-SRR* and Hilbert fractal structures embedded in the ground plane, which allows better control of the resonance.

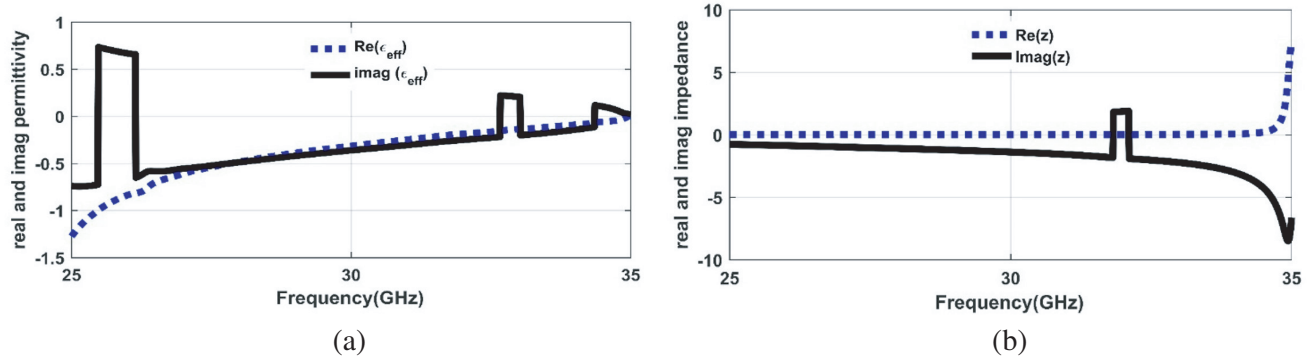


**Figure 6.** The simulated (a) the permeability, (b) the impedance of the metamaterial unit cell Hilbert fractal.

### 3.2. Antenna Design Descriptions

#### 3.2.1. Materials

Printed antenna technology could contribute to the growth of industry and commerce if a low-cost substrate is utilized. However, the use of printed antenna technology can pose significant challenges, especially concerning millimeter-wave radiation. These challenges include metal loss, dielectric losses, stray radiation caused by power lines, and losses due to surface wave modes. Notably, as the frequency increases, the metal loss also rises (measured in nepers per meter). The following formula can be employed to quantify the amount of metal lost along a microstrip line:

$$\alpha_c = \frac{\pi\mu_0 f}{Z_0 W} \delta_s \quad (9)$$

$Z_0$  is the characteristic impedance,  $W$  the line width, and  $\delta_s$  the skin depth.

In the millimeter-wave frequency range, electrical losses are influenced by both frequency and tangency. It is imperative to accurately calculate all losses within this range. Up to 100 GHz, substrates must be characterised, although substrates can be characterised using a variety of techniques. Transmission line methods [1, 2], coaxial probe [1], high Q open resonant cavity [3, 4], use of free space [5, 6], printed resonant circuits can be used to accurately calculate the dielectric constant and loss tangent. The latter technique can be used to select suitable substrates for printed antennas. Surface-mode loss is particularly important in the millimetre-wave spectrum because of the relationship between the thickness of a substrate and its operating wavelength. Indeed, some authors [9, 10] have addressed this issue and provided data on the efficiency of patch antennas as a function of the dielectric substrate. Consequently, the efficiency can be calculated using the formula below:

$$\eta = 1 - \sqrt{\epsilon_r - 1} \frac{h}{\lambda} \left[ 3.4 - \frac{370}{\epsilon_r} \left( \frac{h}{\lambda} \right)^2 \right] \quad (10)$$

In order to build millimeter-scale printed antennas, it seems important to use a substrate with low permittivity and thickness. On the other hand, substrates with a high dielectric constant are suitable for bonding active components and can therefore be used to print a feed network for antenna arrays.

#### 3.2.2. Methods

For the antenna design, a continuous substrate is used ( $\epsilon_r = 2.2$ , thickness  $h = 1.57$  mm, and  $\tan \delta = 0.0009$ ). The resonator consists of two parallel and symmetrical copper layers and is easy to manufacture. The new structure offers a very wide frequency range of 4 GHz with negative values of the refractive index of the waves. Figure 2(b) shows the ground plane of the antenna structure. With the same substrate size, Hilbert fractal curves are proposed to realize artificial magnetic materials in the ground plane.

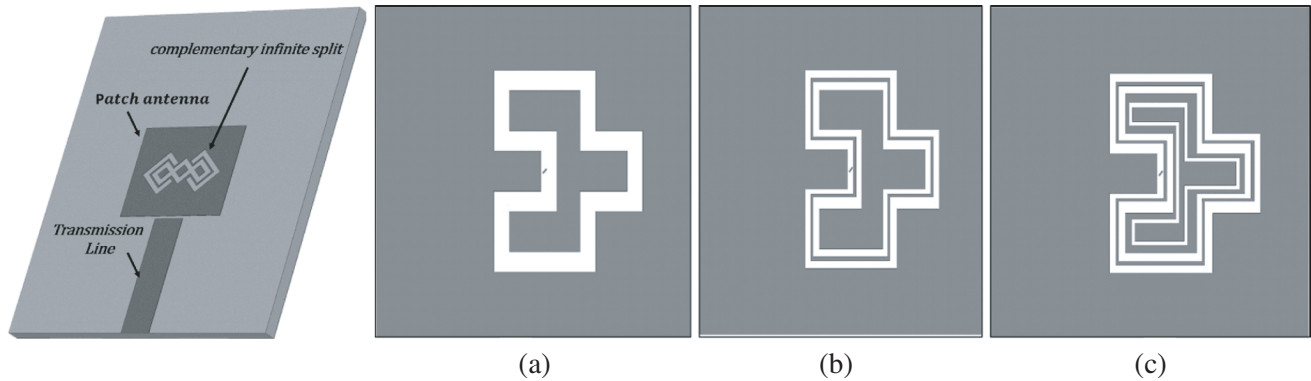


**Figure 7.** Model of proposed antenna, (a) ground plane with fractal Hilbert, (b) ground plane with two fractal Hilbert, (c) ground plane with three fractal Hilbert.

The extracted CI-SRR structure of the rectangular patch is responsible for the broadband frequency. All parameters are presented in Table 1. A substrate of size  $40 \times 25 \text{ mm}^2$  is used; a  $50 \Omega$  line is utilized to feed the patch; and a gap ( $yo$ ) of 0.3 mm is maintained for impedance adaptation. First, we will study the slot effect in the proposed metamaterial. Second, we will treat the effect of the Hilbert fractal on the ground plane. The simulated return loss is shown in Figure 8(a), which operates in the Ka-band and is applicable to 5G communication. The effect of modifying the ground plane by adding a second-order Hilbert fractal increases the bandwidth of the antenna and, also, the value of the gain. On the other hand, the increase of the Hilbert fractal structure in the ground plane allows for the modification of the value of the resonance frequency according to the inverse relation between the electrical length and the resonance frequency, which decreases the size of the electrical length of the patch antenna.

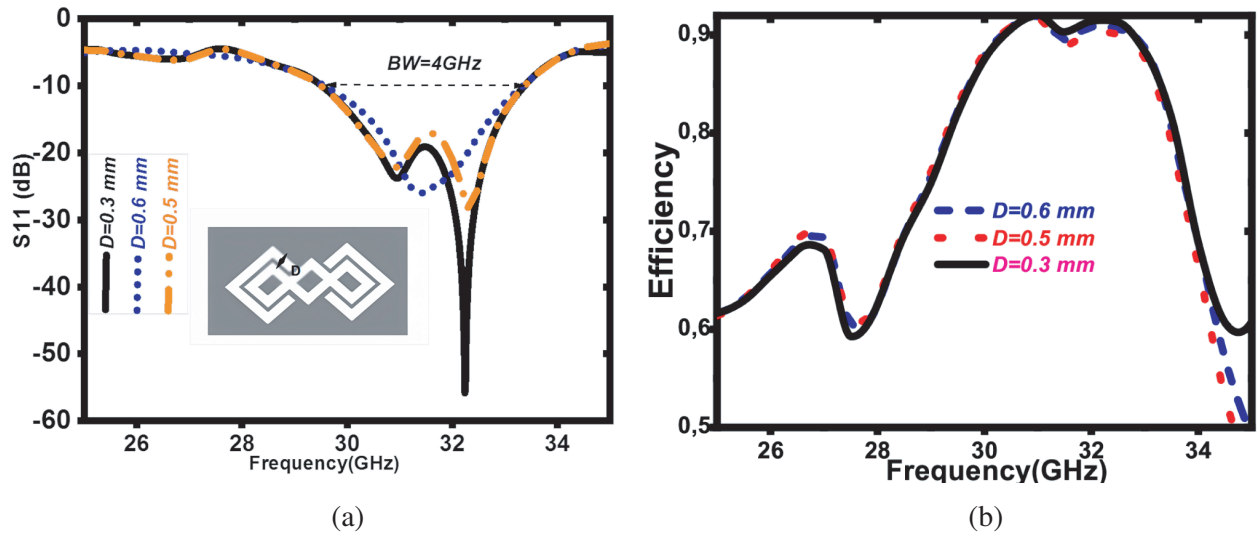


**Figure 8.** (a) The return loss characteristics of the proposed antenna, and (b) the efficiency characteristics of the proposed antenna for different values of  $D$ .

In this part, the effect of slot on the proposed antenna is discussed. It is obvious that the change in slot value affects the return loss, by increasing the slot value, the value of return loss increases, as shown in Figure 8(a). The total simulated efficiency is presented in Figure 8(b). The total efficiency is about 8% in the band 28.512–33.229 GHz which is reliable. The total efficiency is enhanced by utilizing the Rogers RT/Duroid, which is comparatively costly. The gain performs better using the tiny slot, as

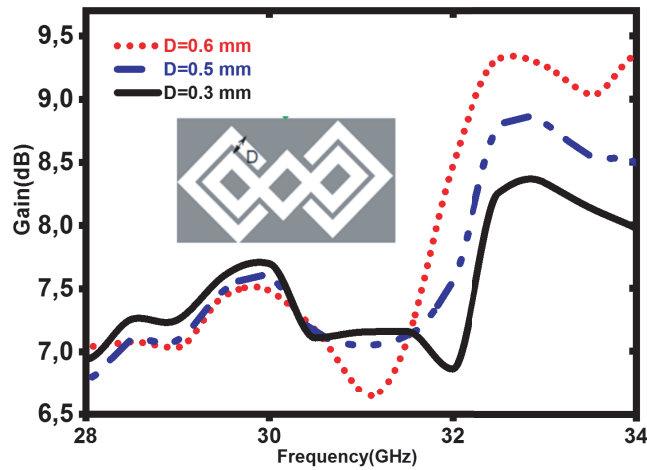


Figure 9. The gain of the proposed antenna different value of  $D$ .

shown in Figure 9. In addition, it increases from 8.4 to 9.5 dB on average over the operating band from 28.512 to 33.229 GHz.

### 3.3. The Effect of Hilbert in Ground Plane

Subsequently, with a fixed value of  $D$  at 0.6 mm, we proceeded to analyze the impact of the ground plane on the antenna performance. By varying the structure of the Hilbert fractal ground plane, depicted in Figure 7, we observed a shift in the resonant frequency. This shift follows an inverse relationship between the electrical length and resonant frequency, as illustrated in Figure 10(a). The depicted figure illustrates the impact of the proposed ground plane structure on the  $S$ -parameters. It reveals an increase in the resonant frequency from 27.06 GHz to 32.78 GHz when incorporating an additional structure alongside the main structure. This improvement in the resonant frequency corresponds to an enhanced bandwidth value, which increases from 3.01 GHz to 4.8 GHz.

Figure 10(b) illustrates the relationship between voltage standing wave ratio (VSWR) and

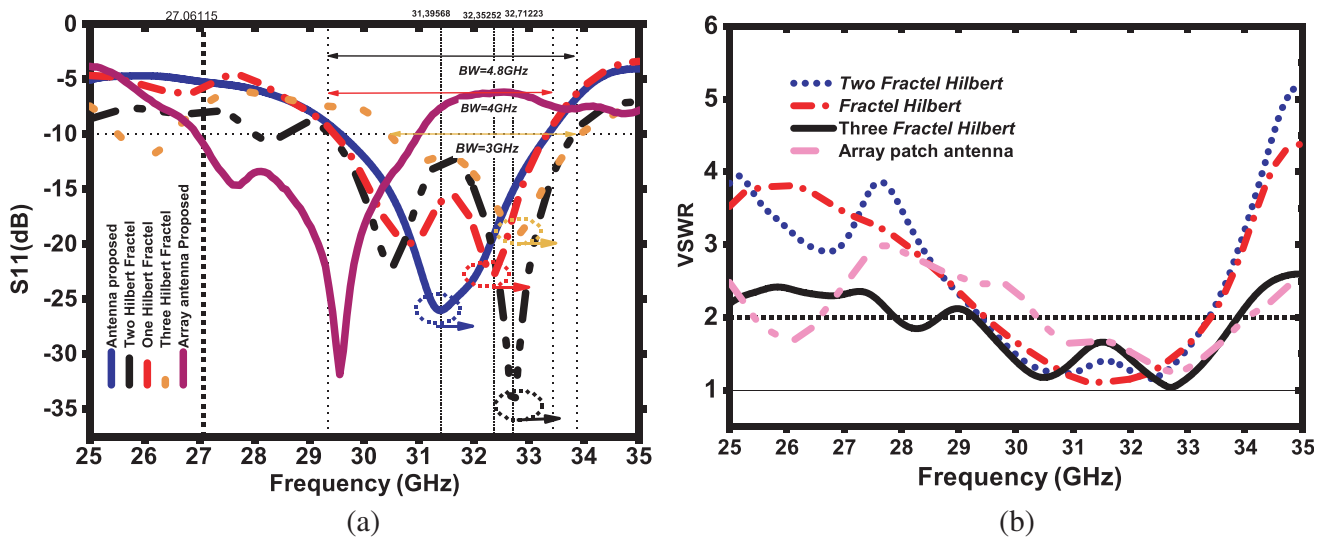
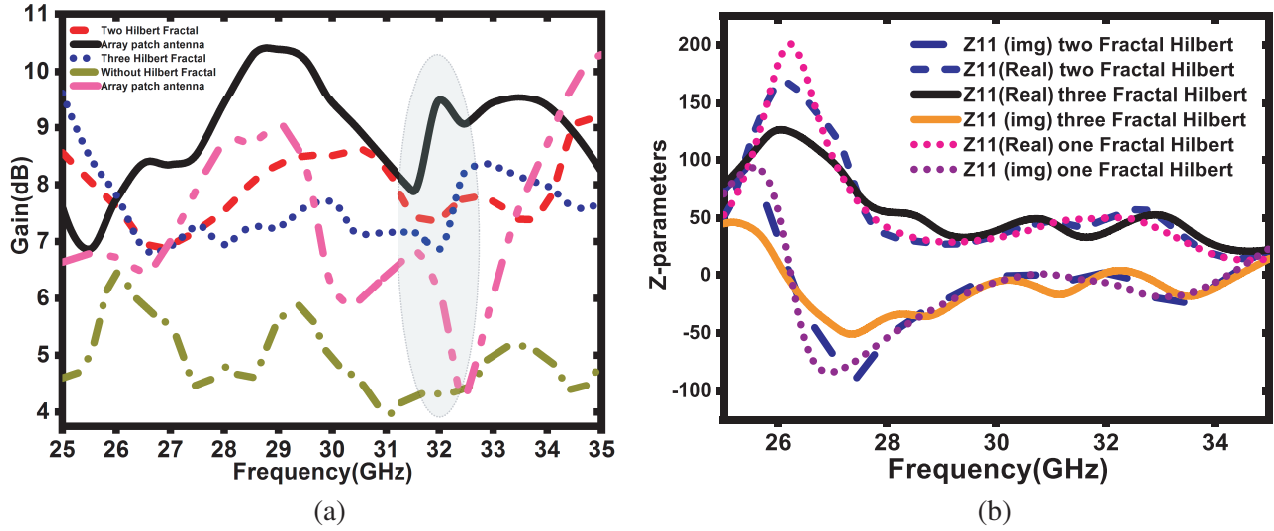
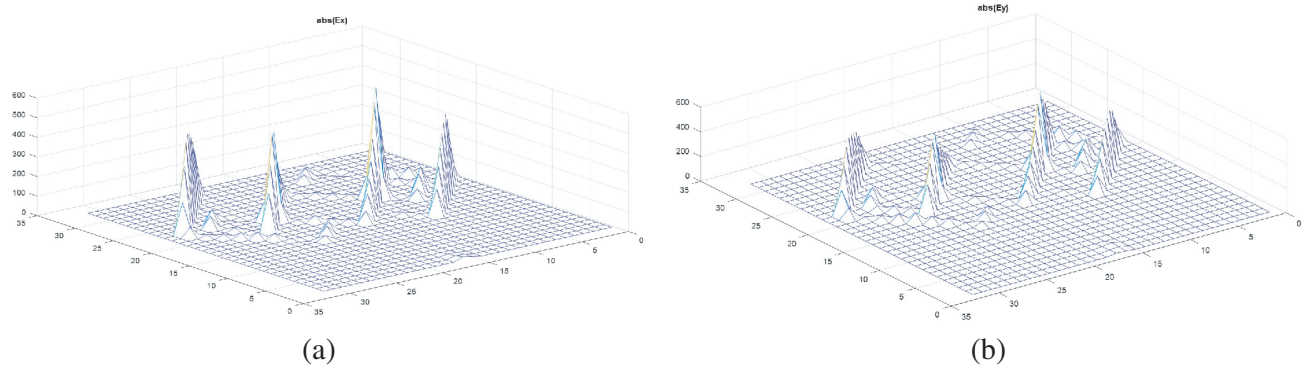


Figure 10. (a) The return loss characteristics, and (b) the VSWR of the proposed antenna depends on Hilbert fractal.



**Figure 11.** (a) The gain of the proposed antenna depends on Hilbert fractal, (b) the  $Z$ -parameters of proposed antenna.



**Figure 12.** 3D plots of the electric fields  $E_x$ ,  $E_y$ , for  $f_r = 32$  GHz and iterations  $n = 1500$ , (a)  $abs(E_y)$ : modulus of the electric field along the  $Ox$  axis, (b)  $abs(E_x)$ : modulus of the electric field along the  $Oy$  axis.

frequency. We observe that the value of this last parameter is between 1 and 2 for frequencies from 31 to 33 GHz. The values of the optimal ground plane dimensions are shown in Table 1. The figure shows that adding the first structural modification enhances the  $S$ -parameters in the frequency range from 31.5 GHz to 32.7 GHz and the bandwidth from 3.7 GHz to 4.7 GHz, with good adaptation ( $S_{11} = -57$  dB). Therefore, the antenna dimensions can be reduced by increasing the number of Hilbert fractals in the ground plane. In addition, the effect on the gain value has increased from 7.5 dB to 9 dB, as shown in Figure 9. The  $Z$ -parameter of the proposed antenna is shown in Figure 11(b). In accordance with the boundary conditions of the circuit interface, the electric field amplitude and current density distribution are shown in Figures 12 and 13 for the optimal ground plane value. In Figure 14, polar coordinates are used to represent these diagrams in the  $E$  and  $H$  planes, respectively. The value of the maximum is 0 dB, obtained in the direction of the maximum, which corresponds to the antenna axis. The surface current distribution for the proposed antenna system is shown below at 32 GHz in Figure 15, note that the current distribution is centered in the proposed CI-SRR and ground plane.

### 3.4. Simulation of the Three Patches

In this part, we will make the same studies as before, putting an accent on the smallest changes.

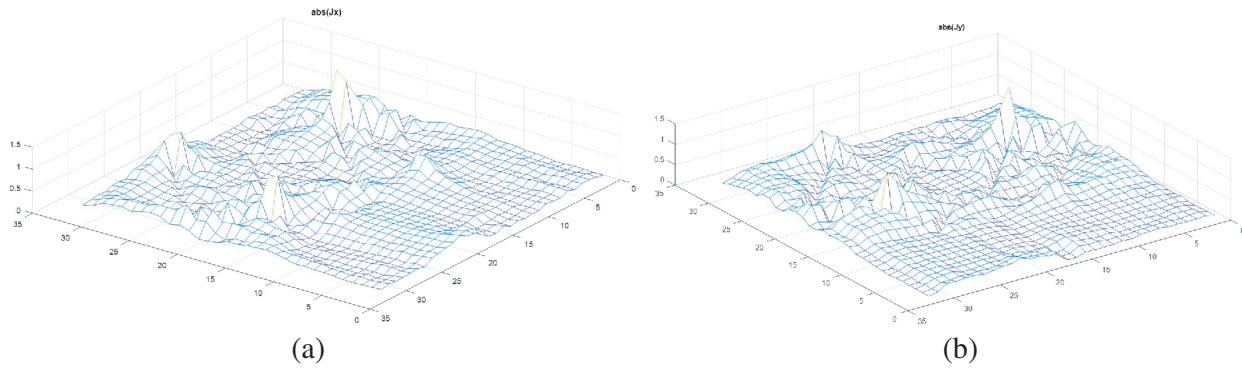


**Figure 13.** 3D plots of the current densities  $J_x, J_y$ , for  $f_r = 32$  GHz and iterations  $n = 1500$ , (a)  $abs(J_x)$ : modulus of the current density along the  $Ox$  axis, (b)  $abs(J_y)$ : modulus of the current density along the  $Oy$  axis.

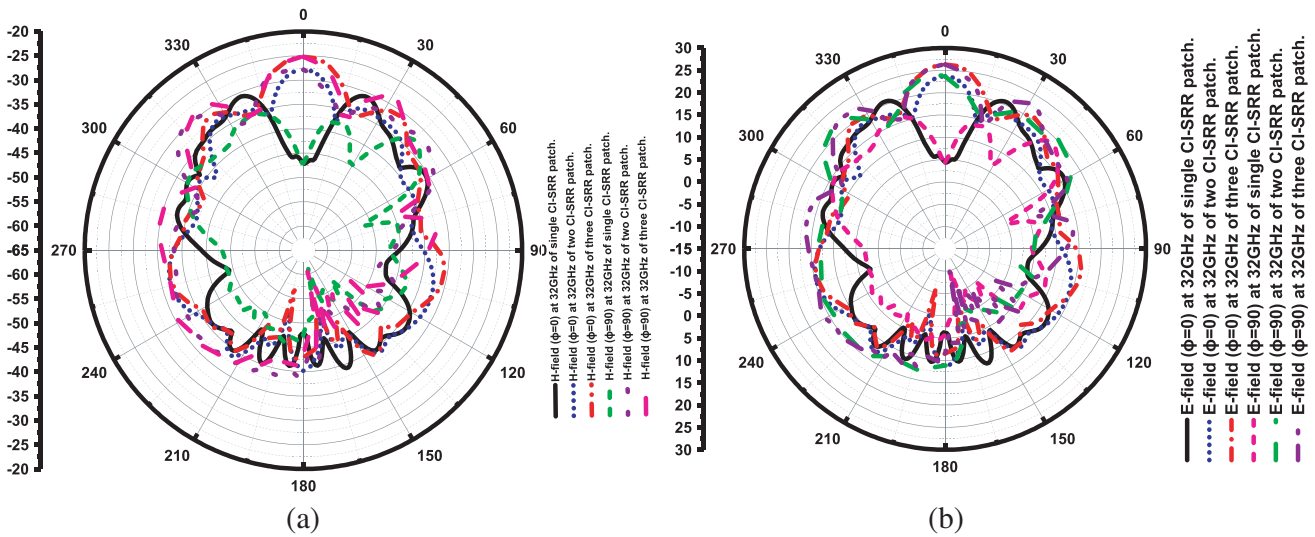


**Figure 14.** Radiation patterns of the proposed antenna at 32 GHz in (a) the H-field and (b) the E-field.

As we illustrated earlier, we will add another patch to the one we just saw. To do this, we create a third patch with the same dimensions as the first. The added patches will also have the same dimensions as the previous ones. Illustrative images are shown in Figure 16. The  $S$ -parameters of the array antenna closely resemble those of the proposed antenna, as illustrated in Figure 10(a). However, a noticeable distinction lies in the size of the antennas. The first configuration illustrates the dimensions of a patch antenna with a total length of 4 cm, while the second configuration shows an array of three patch antennas with a total length of 8 cm. In the second Figure 11(a), it can be seen that the gain value for an antenna array compared to the proposed antenna with a Hilbert fractal in the ground plane is much larger.

#### 4. FABRICATION AND MEASUREMENTS

We constructed the antenna structure on a Rogers RT/Duroid substrate following the presentation of simulation results at WCIP. Figure 17 showcases the fabricated antenna featuring CI-SRR. Additionally, Figure 18 illustrates the simulation and measurement results of the reflection coefficient for the proposed antennas. The  $S$ -parameter measurements of the fabricated prototypes were performed using the PNA-L EYESIGHT N5234B, operating from 10 MHz to 43.5 GHz. For the proposed array antenna, a significant

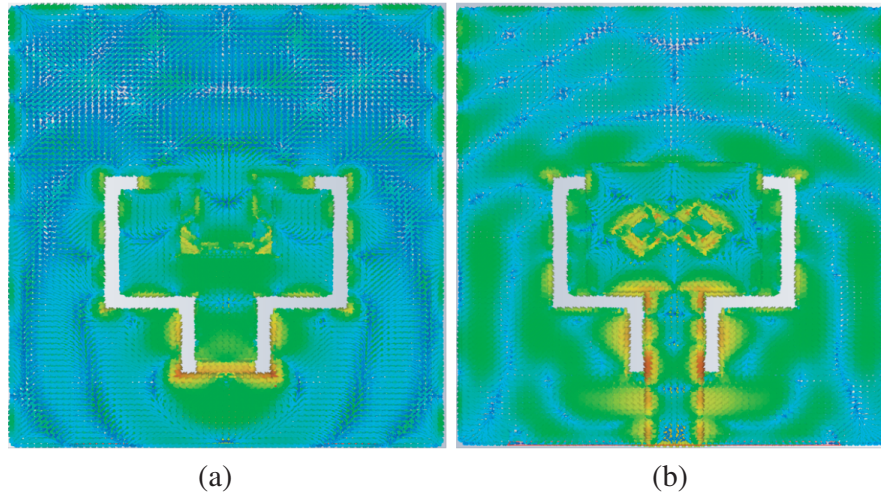


**Figure 15.** The figures depict the current distribution patterns on (a) the CI-SRR patch and (b) the ground plane of the antenna at 32 GHz.

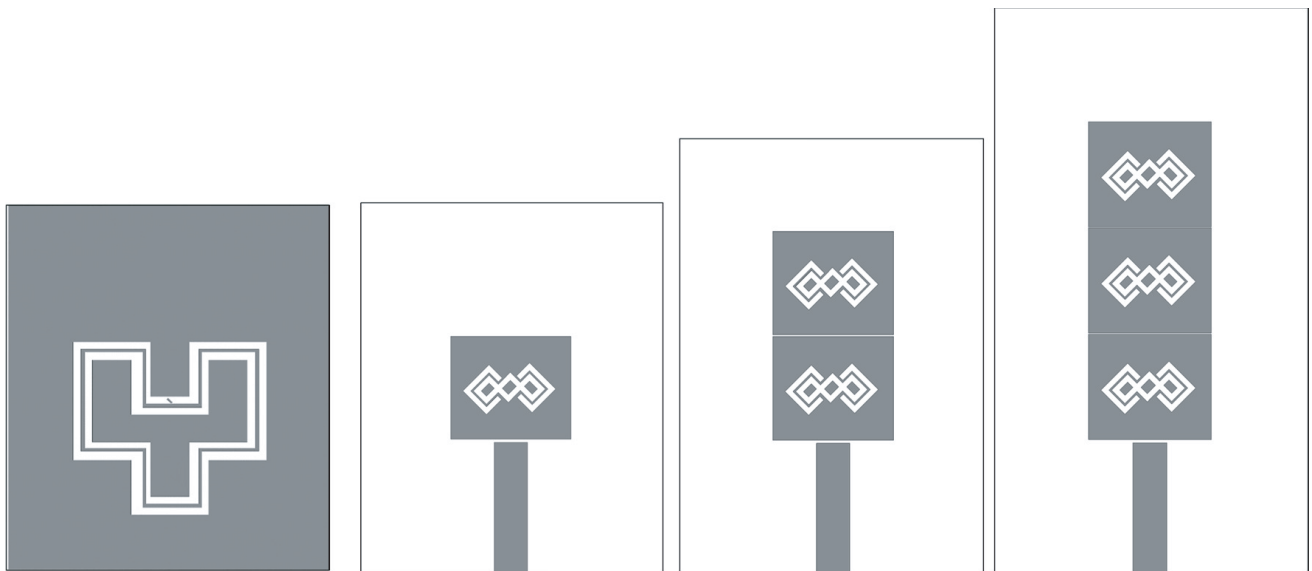


**Figure 16.** The proposed antenna array.

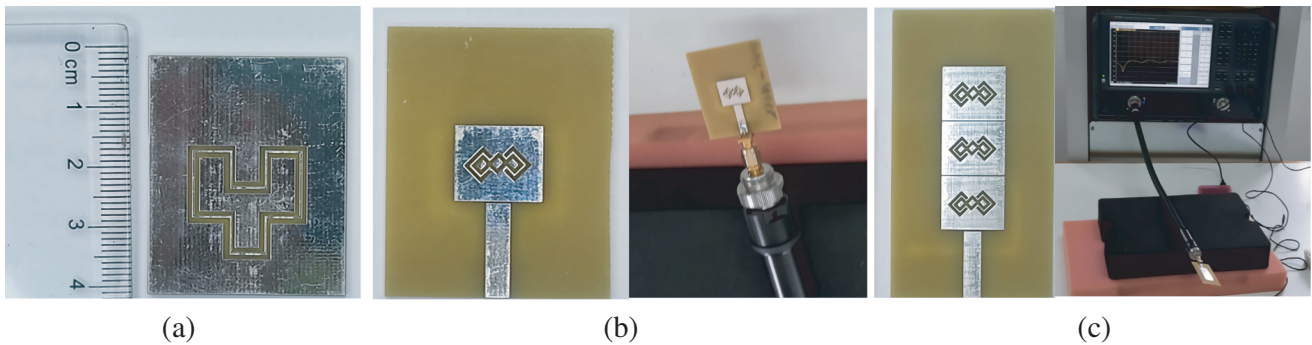


**Figure 17.** The prototype antenna model for the proposed structure, (a) ground plan, (b) patch proposed, (c) array patch.

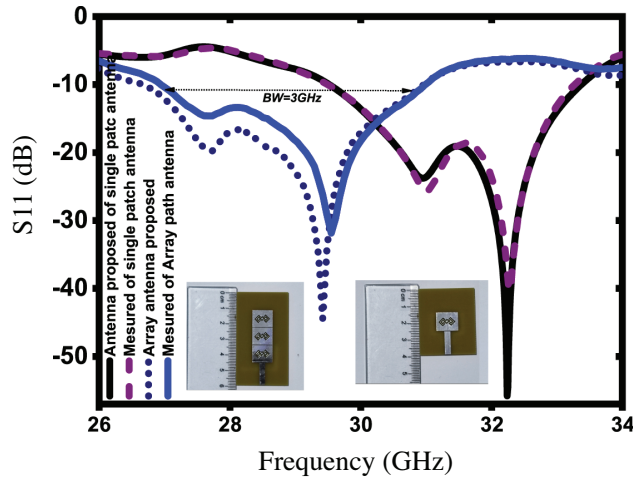


**Figure 18.** The return loss characteristics of the proposed antenna.

reduction was observed; however, the values remained within the required bands. The simulation was planned to cover a frequency range from 29.5 to 33 GHz. The bandwidth ( $-10$  dB) of the measured common impedance spanned from 29 to 33 GHz. The slight discrepancy between the simulation and measurement results can be attributed to changes in substrate permittivity at higher frequencies and manufacturing restrictions imposed by a new product manufacturer. Table 2 compares the performance of the proposed antenna with that of the new generation, which is characterized by its compact size, excellent performance, and ease of manufacture.

**Table 2.** Comparison between the proposed antenna with the recent works.

Ref. design	Antenna type	$f_r$ GHz	Antenna size (mm <sup>2</sup> )	Gain (dBi)	VSWR	BW (GHz)
[41]	Dipole	28	11.3 × 31	10	1.68–2	0.1
[42]	Patch + EBG	24	48 × 31	6	1.6–2.5	2.2
[43]	Cross dipole	28	20 × 27.7	2.2	1–2	3.8
[44]	Patch multilayer	33	27 × 8	11	1.64–2	0.4
[45]	Air filled slot	28	45 × 45	9.7	1–2	0.85
[46]	Dielectric resonator	48	21 × 25	8	1–2.6	1
[47]	L-shaped patch	3.5	75 × 150	3.5	–	0
[48]	elliptically-shaped	3.5	40 × 60	3.86	–	3.5
Proposed work	CI-SRR patch	32	40 × 30	10	1–2	4.8

### 5. CONCLUSION

We introduce a broadband patch antenna design based on a metamaterial that adopts an infinity-shaped patch structure to enhance gain and achieve high isolation for 5G applications. The proposed compact antenna structure utilizes a complementary infinity split ring resonator (CI-SRR) and a Hilbert fractal. These elements are combined on an artificially created meta-surface to create a miniaturized antenna with desired characteristics. The radiator of the antenna is implemented on an RT/Duroid 5880 substrate, enabling excellent performance in high-speed communication systems for 5G. The proposed

patch antenna exhibits wide coverage and high gain. Despite its miniaturized size of  $40 \times 33 \times 1.57 \text{ mm}^2$ , the antenna achieves remarkable performance. With a  $1 \times 3$  array configuration, it offers a broad operational bandwidth of 4.56 GHz, peak gain of 10.5 dBi, and excellent efficiency. These performance metrics have been validated through measured results, confirming the antenna's capabilities.

## ACKNOWLEDGMENT

We extend our sincere gratitude to Rida El Haffar for his invaluable assistance and expert guidance throughout the measurement process in the laboratory.

## REFERENCES

1. Tuyen, V. V., L. Krishnamurthy, S. Qing, and A. Rezazadeh, "3-D low-loss coplanar waveguide transmission lines in multilayer MMICs," *IEEE Transactions on Microwave Theory and Techniques*, Vol. 54, No. 6, 2864–2871, 2006.
2. Mondal, K. and P. Sarkar, "High gain triple-band microstrip patch antenna for WLAN, Bluetooth and 5.8 GHz/ISM band applications," *Wireless Personal Communications*, Vol. 109, No. 6, 2121–2131, 2019.
3. Annou, A., S. Berhab, and F. Chebbara, "Metamaterial-fractal-defected ground structure concepts combining for highly miniaturized triple-band antenna design," *Journal of Microwaves, Optoelectronics, and Electromagnetic*, Vol. 109, No. 2, 212121311, 2019.
4. Mondir, A. and L. Setti, "Metamaterial inspired patch antenna loaded with an interdigital capacitor for wireless applications," *IJMOT*, Vol. 17, 375–384, 2022.
5. Sharma, N. and S. Bhatia, "Edge-coupled parasitic split ring resonator based metamaterial inspired low-cost diamond shaped fractal antenna for multiband wireless applications," *International Journal of Electronics*, Vol. 109, No. 2, 317–336, 2022.
6. Chu, H., J. Chen, S. Luo, and Y. Guo, "A millimeter-wave filtering monopulse antenna array based on substrate integrated waveguide technology," *IEEE Transactions on Antennas and Propagation*, Vol. 64, No. 1, 166–321, 2016.
7. Chen, W. and Y. Lin, "Design of  $2 \times 2$  microstrip patch array antenna for 5G C-band access point applications," *IEEE International Workshop on Electromagnetics: Applications and Student Innovation Competition (iWEM)*, Nagoya, Japan, 2018,
8. Chen, W. and Y. Lin, "Dual-band millimeter-wave microstrip patch array antenna for 5G smartphones," *International Conference on Advanced Science and Engineering (ICOASE)*, 181–185, Zakho, Duhok, Iraq, 2019.
9. Kakkar, A., M. Nirdosh, R. Tripathy, and K. Singh, "Design and analysis of slotted antenna array for 5G application," *2017 Progress In Electromagnetics Research Symposium — Fall (PIERS — FALL)*, Singapore, 2017.
10. Bembarka, A., L. Setti, A. Tribak, and H. Tizyi, "Design of flower-shaped high-efficiency compact UWB antenna," *ITM Web of Conferences*, Vol. 48, 01011, 2022.
11. Bembarka, A., A. Tribak, H. Nachouane, and L. Setti, "Tunable monopole antenna in the sub-6 GHz spectrum for picocell base stations," *Proceedings of the 13th International Conference on Intelligent Systems*, Vol.52, 1–5, 2022.
12. Anouar, M. and S. Larbi, "A new PIFA antenna for future mobile and wireless communication," *E3S Web of Conferences*, Vol. 351, No. 01085, 1–8, 2022.
13. Anouar, M. and S. Larbi, "PIFA Antenna for future mobile 5G," *Proceedings of the 3rd International Conference on Smart City Applications*, Vol. 31, 1–5, 2018.
14. Anouar, M. and S. Larbi, *Array Antenna for Wireless Communication 5G*, Vol. 31, 931–939, Springer International Publishing, 2018.
15. Mondir, A. and L. Setti, "Antenna with Defected Ground Structure for future mobile and Wireless communication 5G," *Proceedings of the Third International Conference on Computing and Wireless Communication Systems*, 2019.

16. Veselago, V., L. Braginsky, V. Shklover, and C. Hafner, "Negative refractive index materials," *Journal of Computational and Theoretical Nanoscience*, Vol. 3, No. 2, 189–218, 2006.
17. Jafari, F., M. Naderi, A. Hatami, and F. B. Zarrabi, "Microwave Jerusalem cross absorber by metamaterial split ring resonator load to obtain polarization independence with triple band application," *AEU International Journal of Electronics and Communications*, Vol. 101, 138–144, 2019.
18. Islam, M. T., M. M. Islam, M. Samsuzzaman, and M. R. I. Faruque, "A negative index metamaterial-inspired UWB antenna with the integration of complementary SRR and CLS unit cells for microwave imaging sensor applications," *Sensors*, Vol. 15, No. 5, 11601–611627, 2015.
19. Lizzi, L., R. Azaro, G. Oliveri, and A. Massa, "Multiband fractal antenna for a wireless communication system for emergency management," *Journal of Electromagnetic Waves and Application*, Vol. 26, No. 1, 1–11, 2013.
20. Laila, D., R. Sujith, V. Shameena, A. Nijas, and A. sujith, "Complementary split ring resonator-based microstrip antenna for compact wireless applications," *Microwave and Optical Technology Letters*, Vol. 55, No. 4, 814–816, 2012.
21. Hu, J. and J. Li, "Compact microstrip antennas using SRR structure ground plane," *Microwave and Optical Technology Letters*, Vol. 56, No. 1, 117–120, 2014.
22. Cao, W., B. Zhang, A. Liu, A. Yu, T. Guo, and Y. Wei, "Gain enhancement for broadband periodic end-fire antenna by using split ring resonator structures," *IEEE Transaction on Antenna and Propagation*, Vol. 60, No. 7, 3513–3516, 2012.
23. Mishra, P., S. Pattnaik, and B. Dhaliwal, "Square-shaped fractal antenna under metamaterial loaded condition for bandwidth enhancement," *Progress In Electromagnetics Research C*, Vol. 78, 3513–3516, 2017.
24. Kuhestania, H., M. Rahimi, Z. Mansouri, F. Zarrabi, and R. Ahmadian, "Design of compact patch antenna based on metamaterial for WiMAX applications with circular polarization," *Microwave and Optical Technology Letters*, Vol. 57, No. 2, 357–360, 2015.
25. Sharma, N. and S. Bhatia, "Split ring resonator based multiband hybrid fractal antennas for wireless applications," *AEU International Journal of Electronics and Communications*, Vol. 93, 39–52, 2018.
26. Patel, S., K. Shah, and Y. Kosta, "Frequency-reconfigurable and high-gain metamaterial microstrip-radiating structure," *Waves in Random and Complex Media*, Vol. 29, No. 3, 523–539, 2019.
27. Sharma, N. and S. Bhatia, "Metamaterial inspired fidget spinner shaped antenna based on parasitic split ring resonator for multi standard wireless applications," *Journal of Electromagnetic Waves and Applications*, Vol. 34, No. 10, 1471–1490, 2020.
28. Sharma, N. and S. Bhatia, "Edge-coupled parasitic split ring resonator based metamaterial inspired low-cost diamond shaped fractal antenna for multiband wireless applications," *International Journal of Electronics*, Vol. 109, No. 2, 317–336, 2022.
29. Yousefi, L. and M. Ramahi, "New artificial magnetic materials based on fractal Hilbert curves," *Proc. IWAT07s*, 237–240, 2007.
30. Krzysztofik, J. and M. Ramahi, "Fractals in antennas and metamaterials applications," *Fractal Analysis: Applications in Physics, Engineering and Technology*, 953–978, 2017.
31. Brambila, F., *Fractals in Antennas and Metamaterials*, IntechOpen, Rijeka, Croatia.
32. Krzysztofik, W. and T. Cao, "Metamaterials in application to improve antenna parameters," *Metamaterials and Metasurfaces*, Vol. 12, No. 2, 63–85, 2018.
33. Ramos, G. L., C. E. Capovilla, H. X. Araújo, C. G. Rego, I. R. Casella, and P. T. Pereira, "A novel FDTD/WP-PML/NUFFT algorithm applied to the design of a printed metamaterial enhanced antenna," *AEU-International Journal of Electronics and Communications*, Vol. 70, No. 9, 1187–1191, 2016.
34. Cui, T., "Electromagnetic metamaterials: Recent advances on the theory, experiments, and applications," *International Conference on Microwave Technology and Computational*, 12–13, 2009.

35. Hrabar, S., D. Bonafacic, and D. Muha, "Application of wire-based metamaterials for antenna miniaturization," *3rd European Conference on Antennas and Propagation (EuCAP)*, 620–623, 2009.
36. Shelby, R. A. and D. R. Smith, "Experimental verification of a negative index of refraction," *Science*, Vol. 292, No. 5514, 77–79, 2001.
37. Pendry, J. B., "Negative refraction makes a perfect lens," *Physical Review Letters*, Vol. 85, No. 3966, 3966–3984, 2000.
38. Ren, Z., Y. Chang, Y. Ma, K. Shih, B. Dong, and C. Lee, "Leveraging of MEMS technologies for optical metamaterials applications," *Fractal Analysis — Applications in Physics, Engineering and Technology*, Vol. 8, No. 3, 1900653–190066, 2020.
39. Krzysztofik, J. W. and D. R. Smith, "Fractals in antennas and metamaterials applications," *Fractal Analysis — Applications in Physics, Engineering and Technology*, 978–953, 2017.
40. Mondir, A., L. Setti, and R. El Haffar, "Design analysis, and modeling using WCIP method of novel microstrip patch antenna for THz applications," *Progress In Electromagnetics Research C*, Vol. 125, 67–82, 2022.
41. Iqbal, A., B. Abdul, S. Amor, M. Nazih, I. Elfergani, and R. Jonathan, "Electromagnetic bandgap backed millimeter-wave MIMO antenna for wearable applications," *IEEE Access*, Vol. 7, No. 1, 111135–111144, 2019.
42. Lin, W., R. Ziolkowski, B. Thomas, "28 GHz compact omnidirectional circularly polarized antenna for device-to-device communications in the future 5G systems," *IEEE Transactions on Antennas and Propagation*, Vol. 65, No. 12, 6904–6914, 2017.
43. Ullah, U., M. Al-Hasan, K. Slawomir, and I. Mabrouk, "Series-slot-fed circularly polarized multiple-input-multiple-output antenna array enabling circular polarization diversity for 5G 28 GHz indoor applications," *IEEE Transactions on Antennas and Propagation*, Vol. 69, No. 9, 5607–5616, 2021.
44. Usman, M., K. Enis, J. Nasir, Z. Yuanwei, Y. Chao, and A. Zhu, "Compact SIW fed dual-port single element annular slot MIMO antenna for 5G mmWave applications," *IEEE Access*, Vol. 9, No. 9, 91995–92002, 2021.
45. Usman, M., K. Enis, J. Nasir, Z. Yuanwei, Y. Chao, and A. Zhu, "A MIMO dielectric resonator antenna with improved isolation for 5G mm-wave applications," *IEEE Access*, Vol. 9, No. 9, 91995–92002, 2021.
46. Sharawi, M., S. Podilchak, M. Hussain, T. Mohamed, and A. Yahia, "Dielectric resonator based MIMO antenna system enabling millimetre-wave mobile devices," *IET Microwaves, Antennas & Propagation*, Vol. 11, No. 2, 287–293, 2017.
47. Alhaqbani, H., M. Bait-Suwailam, A. Aldhaeabi, and S. Almoneef, "Wideband diversity MIMO antenna design with hexagonal slots for 5G smart mobile terminals," *Progress In Electromagnetics Research C*, Vol. 120, No. 2, 105–117, 2022.
48. Bait-Suwailam, M., S. Almoneef, and S. Saeed, "Wideband MIMO antenna with compact decoupling structure for 5G wireless communication applications," *Progress In Electromagnetics Research C*, Vol. 120, No. 2, 117–125, 2021.